ACS Energy LETTERS

http://pubs.acs.org/journal/aelccp

LETTER

Single Pass CO_2 Conversion Exceeding 85% in the Electrosynthesis of Multicarbon Products via Local CO_2 Regeneration

Colin P. O'Brien,[‖] Rui Kai Miao,[‖] Shijie Liu, Yi Xu, Geonhui Lee, Anthony Robb, Jianan Erick Huang, Ke Xie, Koen Bertens, Christine M. Gabardo, Jonathan P. Edwards, Cao-Thang Dinh, Edward H. Sargent, and David Sinton*

Cite This: *ACS Energy Lett.* 2021, 6, 2952–2959

Read Online

ACCESS | Metrics & More | Article Recommendations | Supporting Information

ABSTRACT: The carbon dioxide reduction reaction (CO_2RR) presents the opportunity to consume CO_2 and produce desirable products. However, the alkaline conditions required for productive CO_2RR result in the bulk of input CO_2 being lost to bicarbonate and carbonate. This loss imposes a 25% limit on the conversion of CO_2 to multicarbon (C_{2+}) products for systems that use anions as the charge carrier—and overcoming this limit is a challenge of singular importance to the field. Here, we find that cation exchange membranes (CEMs) do not provide the required locally alkaline conditions, and bipolar membranes (BPMs) are unstable, delaminating at the membrane−membrane interface. We develop a permeable CO_2 regeneration layer (PCRL) that provides an alkaline environment at the CO_2RR catalyst surface and enables local CO_2 regeneration. With the PCRL strategy, CO_2 crossover is limited to 15% of the amount of CO_2 converted into products, in all cases. Low crossover and low flow rate combine to enable a single pass CO_2 conversion of 85% (at 100 mA/cm^2), with a C_{2+} faradaic efficiency and full cell voltage comparable to the anion-conducting membrane electrode assembly.

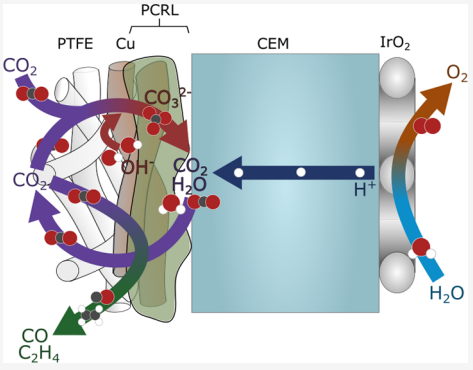

The electrochemical CO_2 reduction reaction (CO_2RR) presents an opportunity to utilize renewable electricity to produce chemical fuels and feedstocks from CO_2.[1,2] Valuable multicarbon (C_{2+}) products, such as ethylene (C_2H_4) and ethanol (C_2H_5OH), are of particular interest in view of large existing markets.[3] Providing reactant CO_2 gas directly to the catalyst sites with gas diffusion electrodes (GDEs) enables CO_2RR systems to attain impressive reaction rates ($\gg$ 100 mA/cm^2).[4,5]

Membrane electrode assembly cells combine GDEs and membranes in a zero-gap fashion. This configuration mitigates electrolyte degradation and salt precipitation issues characteristic of alkaline flow cells.[6−9] Alkaline conditions are required at the cathode[10] to suppress the hydrogen evolution reaction (HER) and enable a high faradaic efficiency (FE) toward CO_2RR products.[11,12] Locally, alkaline conditions are maintained during CO_2RR by hydroxide anions produced at the catalyst layer (eqs 1 and 2). However, these conditions result in the competing reaction of CO_2 with hydroxide forming bicarbonate and carbonate (eqs 3 and 4).[13] These ions electromigrate through the anion exchange membrane (AEM) to the anode where they combine with protons generated by the anodic oxygen evolution reaction to form CO_2 and water.[13] Here, the CO_2 bubbles out of the locally acidic anolyte and combines with produced oxygen, rendering a gas mixture that is costly to separate.[14] This crossover of CO_2 in MEA systems results in a low single pass conversion for CO_2RR.

When carbonate is the dominant charge carrier through the AEM, CO_2 conversion efficiency is limited to 50% in the production of CO.[15−17]

$$CO_2 + H_2O + 2e^- \rightarrow CO + 2OH^- \quad (1)$$

$$2CO_2 + 8H_2O + 12e^- \rightarrow C_2H_4 + 12OH^- \quad (2)$$

$$CO_2 + OH^- \rightarrow HCO_3^- \quad (3)$$

$$CO_2 + 2OH^- \rightarrow CO_3^{2-} + H_2O \quad (4)$$

Received: June 1, 2021
Accepted: July 23, 2021

https://doi.org/10.1021/acsenergylett.1c01122
ACS Energy Lett. 2021, 6, 2952–2959

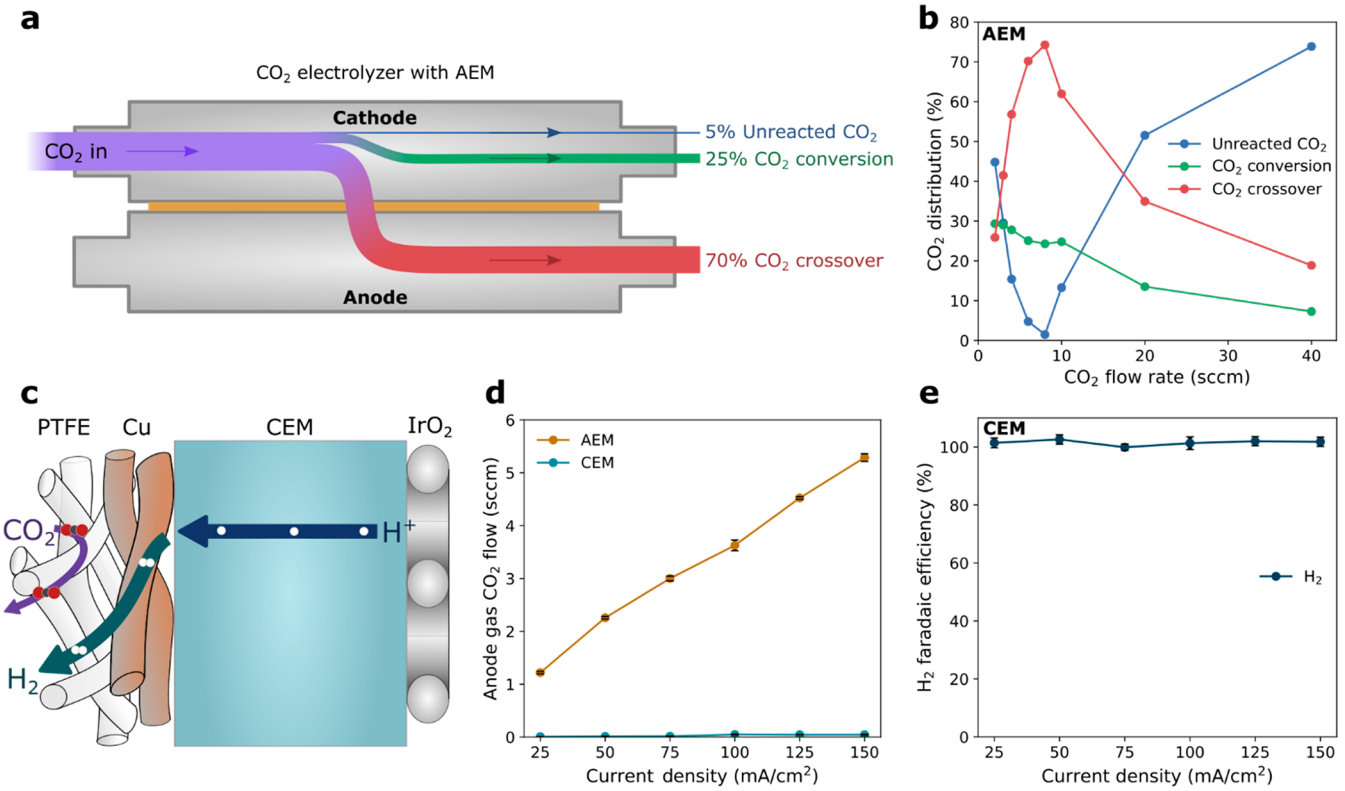

Figure 1. CO_2 reactant loss in a conventional AEM electrolyzer and performance in a CEM electrolyzer. (a) Schematic of an AEM cell showing the flow distribution of CO_2 with a Cu catalyst operating at 150 mA/cm^2 and 6 sccm of CO_2 flow. (b) CO_2 distribution in the AEM cell at 150 mA/cm^2. (c) Schematic of species transport within the MEA with a CEM. (d) Comparison of the anode gas CO_2 flow rate of an MEA with an AEM and an MEA with a CEM as a function of current density. (e) Faradaic efficiency (FE) of the MEA with a CEM, no CO_2RR products are detected. Error bars represent the standard deviation of at least three measurements under the same conditions.

Compared to CO production, C_{2+} production requires more electrons to be transferred through the membrane per molecule of CO_2 converted (eqs 1 and 2): the dominant C_2 products on a multicrystalline Cu catalyst, C_2H_4 and C_2H_5OH, both require six electrons per CO_2 molecule converted. With a carbonate charge carrier, three molecules of CO_2 will be transported through the membrane for each molecule of CO_2 converted to C_2H_4 or C_2H_5OH, limiting the CO_2 conversion efficiency to a maximum of 25%. A low CO_2 conversion efficiency necessitates energy-intensive gas separation to recover unreacted CO_2 from both the cathodic and anodic gas product streams,[18] and the associated costs render electrocatalytic CO_2 conversion processes unviable. Going beyond this conversion limit is a critical challenge for the field.[17]

Here, we begin from a reference cell based on prior reports—we demonstrate that the Cu cathode MEA cell with an AEM has a prohibitively low CO_2 conversion efficiency. We assemble an MEA with a cation exchange membrane (CEM) to reduce the CO_2 transport to the anode; however, the environment provided by the CEM configuration leads exclusively to H_2 production. We show that a cell with a forward-bias bipolar membrane (BPM) can provide an alkaline environment conducive to C_2H_4 production; however, the delamination of the membranes leads to poor stability even at a low current density.

We sought a means to simultaneously impede proton transport and facilitate the local regeneration of CO_2. We engineered a permeable CO_2 regeneration layer (PCRL) that shields the cathode from protons and enables the local regeneration of CO_2 for subsequent reaction. When coupled to a CEM, the PCRL provides a product distribution similar to the conventional AEM cell; the PCRL coupled CEM cell reaches 40% FE toward C_2H_4 and 55% FE toward C_{2+} products. With the PCRL cell configuration, we attain 85% CO_2 conversion efficiency.

We assembled an AEM MEA cell (Sustainion X37-50) with a cathode consisting of a porous polytetrafluoroethylene (PTFE) gas diffusion layer (GDL) sputtered with a 250 nm Cu catalyst layer. We then applied a stabilizing carbon layer and a conductive graphite layer.[7,12] While operating the cell at 150 mA/cm^2, we varied the flow rate of the CO_2 fed into the cell while measuring the flow rate and composition of the cathode and anode gas and liquid products (Figure 1B). At flow rates of 20 and 40 sccm, there was sufficient mass transport of CO_2 to the catalyst, evidenced by the low 7% H_2 FE (Figure S1); however, the total amount of input CO_2 converted to products was less than 15%. At flow rates between 6 and 10 sccm, CO_2 mass transport became limiting, and the HER increased from 8% FE at 10 sccm to 20% FE at 6 sccm. The unreacted CO_2 in the outlet stream reached a minimum value of 1% of that of inlet CO_2 (8 sccm). The CO_2 conversion reached its maximum between 25 and 30% (exceeding the established conversion limit for C_2 production due to a small amount of C_1 production).

The CO_2 transported through the membrane matched that predicted for the case of carbonate as the sole charge carrier. The resulting anode head gas contained a mixture of 60−70 vol % CO_2 and 30−40 vol % O_2. Regenerating a reactable CO_2 stream from this mixture would require an energy-intensive

https://doi.org/10.1021/acsenergylett.1c01122
ACS Energy Lett. 2021, 6, 2952−2959

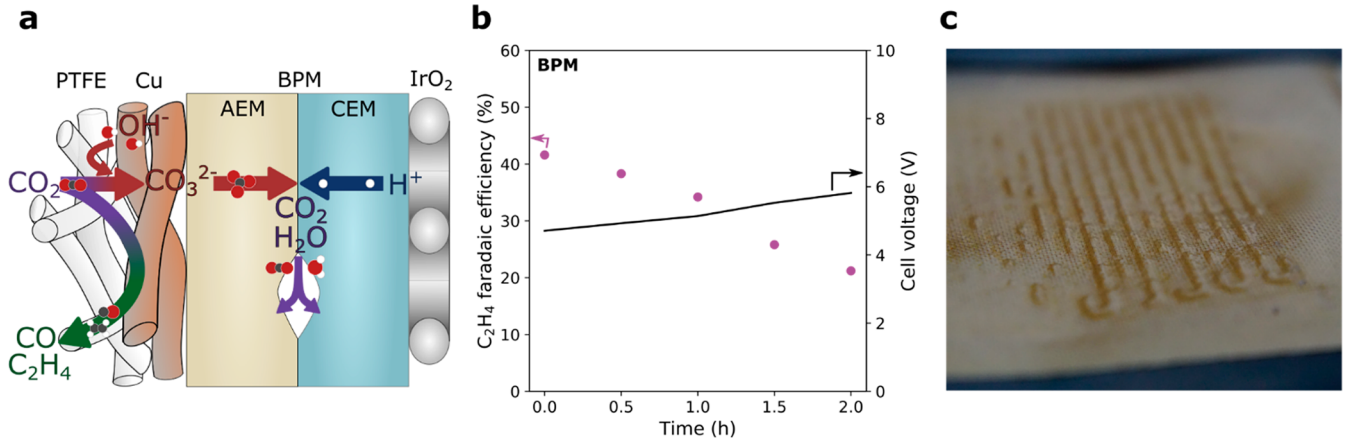

Figure 2. Electrochemical performance in a BPM electrolyzer. (a) Schematic of the species transport within an MEA with a forward bias BPM. (b) C_2H_4 and voltage stability of the forward bias BPM at 50 mA/cm^2. (c) A picture of the BPM after running in the forward bias for 2 h at 50 mA/cm^2. The membrane blistered at the AEM:CEM interface in the areas under the flow channels of the cell.

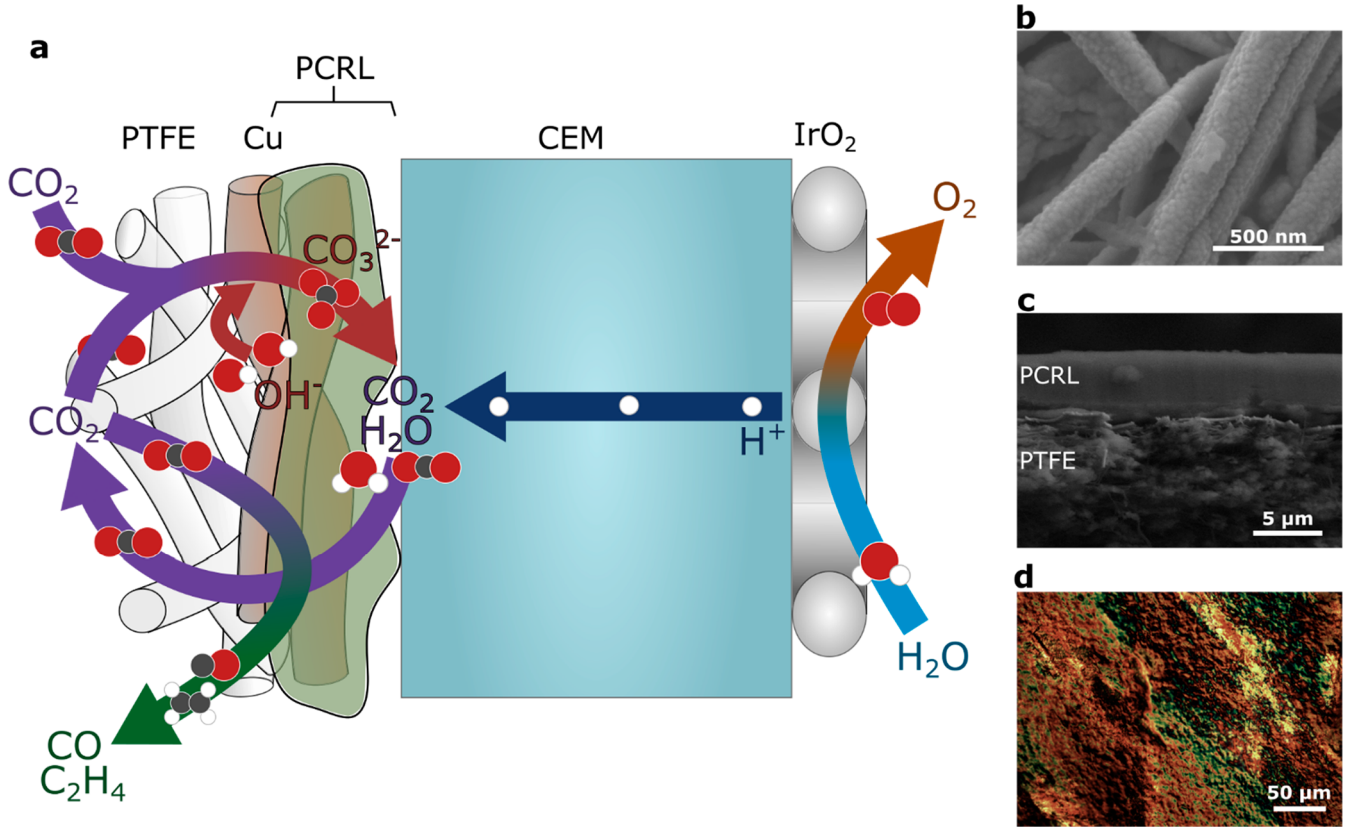

Figure 3. The permeable CO_2 regeneration layer. (a) Schematic of the transport and reactions within the MEA. (b) SEM of the sputtered Cu on the PTFE cathode surface without any coating. (c) Cross-section SEM of the cathode with 1.5 mg/cm^2 coating. (d) Optical microscope image of the cathode surface with 1.5 mg/cm^2 coating at 10× magnification.

chemical absorption separation process (e.g., monoethanolamine CO_2 absorption).[19]

Incorporating a CEM in the place of the AEM blocks carbonate transport to the anode.[20] We assembled an MEA with a CEM (Nafion 117) and measured the CO_2RR performance. Deionized water was employed as the anolyte to ensure that protons were the sole charge carrier. The loss of CO_2 was avoided at all current densities (Figure 1d), but the cathode environment was too acidic for efficient CO_2RR at current densities greater than 25 mA/cm^2 (Figure 1e).[21−25] The acidic cathode environment improves HER kinetics and worsens CO_2RR kinetics (Figure S3); therefore, HER dominates in the CEM configuration.

Pairing anion and cation selective membrane layers in a BPM is another approach to block reactant and product crossover in electrolyzers.[15,20] With the CEM adjacent to the cathode (in a conventional reverse-bias BPM configuration), the cathode becomes acidic due to the influx of protons and, as in the CEM electrolyzer, is not productive in the CO_2RR without an additional buffer layer.[26,27] An alkaline environment at the cathode can be achieved in a conventional forward-bias

https://doi.org/10.1021/acsenergylett.1c01122
ACS Energy Lett. 2021, 6, 2952−2959

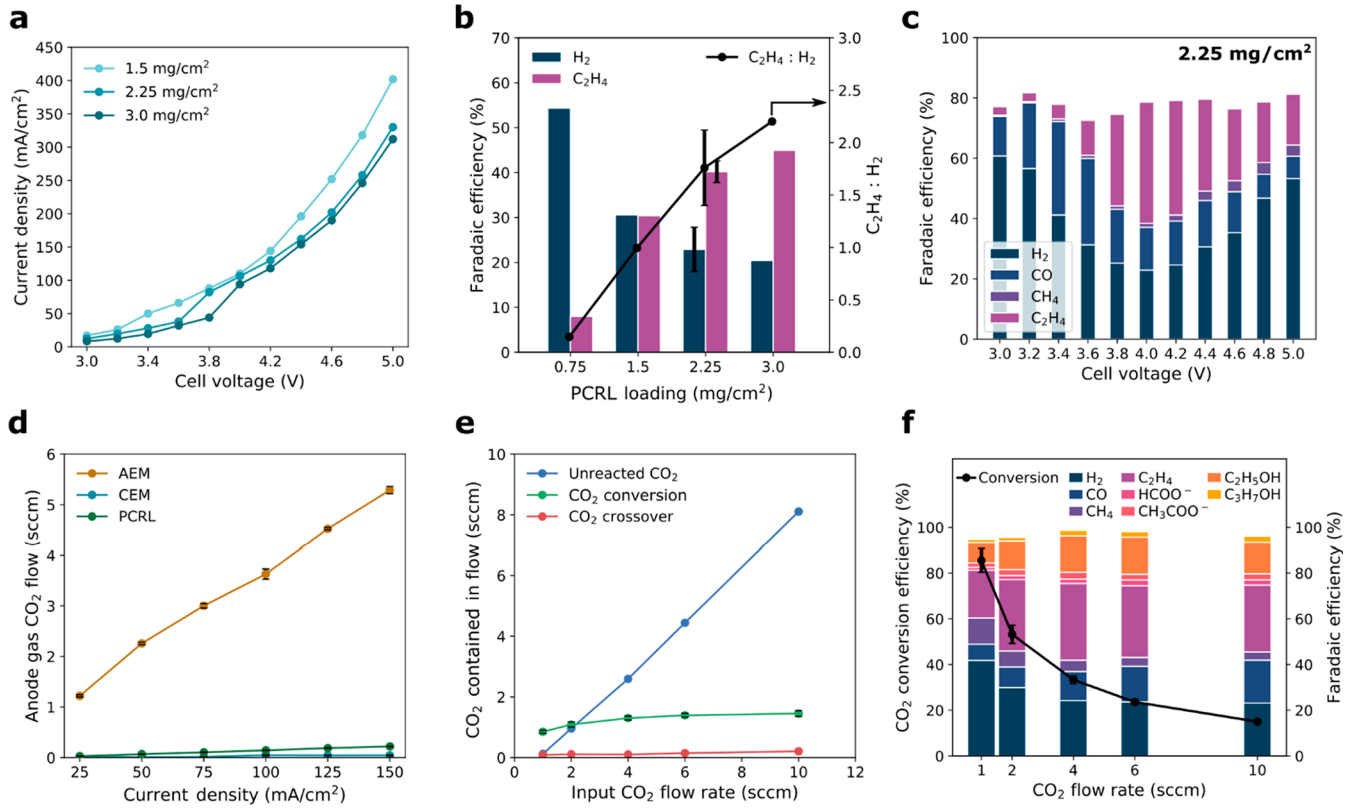

Figure 4. Electrochemical performance of an MEA with a PCRL. (a) Polarization curves with different PCRL loadings on a Cu catalyst. (b) Highest C_2H_4 FE and C_2H_4 to H_2 ratio for each PCRL loading. (c) Gas product FE for a Cu catalyst with a 2.25 mg/cm^2 coating as a function of cell voltage. (d) Anode gas CO_2 flow rate for the PCRL compared to the AEM and CEM cases. (e) CO_2 flow distribution with the 2.25 mg/cm^2 coating as a function of CO_2 flow at 100 mA/cm^2. (f) CO_2 conversion efficiency with 2.25 mg/cm^2 coating as a function of CO_2 flow rate at 100 mA/cm^2. Error bars represent the standard deviation of at least three measurements under the same conditions.

BPM configuration, with the AEM layer adjacent to the cathode.

We performed the CO_2RR with a BPM (Fumasep FBM) in the forward bias at a low current density (50 mA/cm^2, Figure 2a). We observed more CO_2 in the anode gas compared to the CEM case (Figure S4) due to the accumulation and pressure buildup of water and gaseous CO_2 at the membrane junction and subsequent migration to both the cathode and anode sides. The formation of the CO_2 and water at the membrane junction caused the AEM and CEM to delaminate (Figure 2c) and resulted in a loss of ethylene FE within 0.5 h (Figure 2b).[15] The conventional BPM does not provide a solution to the CO_2 conversion challenge because reactant CO_2 is lost to the membrane junction, and the system is unstable even at a low current density (50 mA/cm^2).

We sought a new system design that would block the transport of protons while providing a pathway for regenerated water and gaseous CO_2. We accomplished this via a permeable anion-selective CO_2 regeneration layer that provides alkaline conditions at the catalyst surface, amid acidic conditions provided by a CEM. In this configuration, the CO_2-crossover blocking capability of a BPM is retained, with the distinction that evolved CO_2 remains available for reaction. Reactant CO_2 lost to bicarbonate and carbonate is regenerated locally, and the permeability of the layer allows for the transport of regenerated CO_2 to the catalyst for subsequent reaction (Figure 3a).

The cathode is fabricated by first sputtering Cu on a porous PTFE GDL (Figure 3b), then the PCRL is deposited onto the Cu layer (Figure 3c and d; SEMs in Figure S5). The functional groups of the anion exchange polymer (Aemion AP1-CNN5-00-X) create a positive space charge, enabling the transport of anions and impeding the transport of cations. The polymer coating on the cathode allows for CO_2 transport to the catalyst via diffusion through the water-filled hydrated ionic domains in the polymer matrix.[28,29] The layer is thin, less than 10 μm (Figure 3c), to minimize the obstruction of water and CO_2 from the membrane junction to the catalyst surface.[30]

The CO_2RR typically requires the presence of alkali metal cations in the outer Helmholtz plane to create a reaction environment suitable for efficient conversion.[31−33] However, within the PCRL, the positively charged functional groups in the polymer structure act as a fixed positive charge near the catalyst surface that can stabilize CO_2RR intermediates to promote C−C coupling on Cu catalysts. The quaternary ammonium and heterocyclic (including imidazolium and benzimidazolium) functional groups that are commonly used as the positive charge in anion exchange ionomers[28] have been shown to allow for the intermolecular interaction of water with surface adsorbed CO and promote the hydrogenation of surface bound CO to ethylene.[34−39] The cations contained within the polymer structure of the PCRL (Figure S6) eliminate the need for alkali metal cations in the electrolyte.

To assess the impact of the PCRL on the cathode pH and CO_2 conversion efficiency, we evaluated the electrochemical performance in an MEA cell with a Nafion 117 CEM, an IrO_2 anode, and DI water anolyte (Figure 4). The Nafion 117 CEM was selected to provide a greater thickness than that of the

https://doi.org/10.1021/acsenergylett.1c01122
ACS Energy Lett. 2021, 6, 2952−2959

more commonly applied Nafion XL or Nafion 211 membranes. The thicker CEM provides a larger diffusion barrier to minimize transport of CO_2 through the hydrophobic domains of the Nafion polymer.[40,41] The use of DI water anolyte ensures that protons are the only cations that can transport charge through the CEM. If any salts are present in the anolyte, the associated cations will be transported through the CEM and react with carbonate and bicarbonate to form salts at the junction of the PCRL and CEM, thus preventing CO_2 from being regenerated and recycled to the cathode catalyst. We fabricated cathodes with coatings of different loadings and assessed their performance in an electrolyzer in terms of current, FE, CO_2 crossover, and overall CO_2 conversion efficiency.

We characterized the current−voltage response with loadings of PCRL coating between 1.5 and 3 mg/cm^2 (Figure 4a). The cell voltage was varied from 3 to 5 V, and the samples with lower loadings reached higher currents. The observed differences in current density among the samples is not due to the changes in the ionic conduction because of the relatively constant ohmic resistance (Figure S7). The current response is instead attributed to changes in the local pH at the cathode; a 3 mg/cm^2 loading provides a higher pH, and thus a larger Nernstian pH voltage loss, compared to a 1.5 mg/cm^2 loading. Nernstian loss increases cell voltage by 0.059 V per unit difference in pH between the cathode and anode. For each PCRL loading, we saw a large change in current density once ∼40 mA/cm^2 was reached, corresponding to a change in the reaction mechanism. At current densities less than 40 mA/cm^2, the potential required for protons to pass through the PCRL and be consumed directly in the CO_2RR and HER is less than the potential required to form alkaline conditions at the cathode. At current densities greater than 40 mA/cm^2, the PCRL is not adequately conductive for protons to pass through at a sufficient rate, so it becomes kinetically favorable for water near the catalyst to become the proton donor—leading to a further increase in the pH from the produced hydroxide ions. This effect is confirmed by a one-dimensional multiphysics model that estimated the pH at the cathode as a function of the coating thickness and the current density (Figure S8). This shift was reflected in the current−voltage response (Figure 4a) and corresponded to a higher cathode pH and an increase in C_2H_4 selectivity (Figure S9).

Increasing the PCRL loading from 0.75 mg/cm^2 to 2.25 mg/cm^2 caused the maximum CO_2RR toward C_2H_4 to increase from 8% to 40% FE and the associated HER to decrease from 54% to 23% FE (Figure 4b). The increased coating thickness creates a more effective proton transport barrier, leading to higher pH at the cathode. Increasing the PCRL loading to 3.0 mg/cm^2 only led to a small further increase of the FE for H_2 and C_2H_4 compared to the 2.25 mg/cm^2 layer, which suggests that the local pH at the cathode is not the limiting factor beyond a threshold alkaline pH. The 2.25 mg/cm^2 case exhibited similar currents to the 3 mg/cm^2 layer while showing similar product selectivity. As the voltage was increased from 3.0 to 3.6 V, the FE for H_2 decreased and CO became the major product at 28% FE (Figure 4c). Once the voltage was increased from 3.8 to 4.2 V, the pH at the cathode became high enough for significant C_{2+} production, and the maximum C_2H_4 FE of 40% was reached. Increasing the voltage beyond 4.2 V increased the FE for H_2 due to CO_2 mass transport limitations in the PCRL, an effect observed previously for hydrophilic cathode layers.[40] The 2.25 mg/cm^2 coating provided steady selectivity and cell voltage for 8 h of continuous operation at 100 mA/cm^2 (Figure S12).

To measure the effectiveness of the PCRL coupled CEM in preventing CO_2 loss, we measured the concentration and flow rate of CO_2 in the anode gas (Figure 4d). With the PCRL layer, CO_2 outflow from the anode gas was less than 4% that of the AEM comparison case (i.e., 0.2 sccm with the PCRL, versus >5 sccm with the AEM at the same reaction rate of 150 mA/cm^2). Some CO_2 in the anode gas can be attributed to liquid product crossover and subsequent oxidation (further supported by the 5−10% missing FE, Figure S10). Depending on the liquid product oxidized to CO_2 (e.g., ethanol vs formate), this route could account for 30−100% of the 0.2 sccm of CO_2 measured in the anode tail gas. For all input CO_2 flow rates, the amount of CO_2 that crossed over (Figure 4e) was less than 15% of the amount of CO_2 converted into products (e.g., 0.2 sccm crossover, compared to 1.4 sccm converted). Low crossover enables high CO_2 conversion at flow rates less than 2 sccm. Selectivity was relatively constant at high input CO_2 flow rates (Figure 4f), but below 4 sccm CO_2 mass transport limitations were reached and the FE for H_2 increased. At 1 sccm, a CO_2 conversion efficiency of 85 ± 5% was achieved (with a faradaic efficiency of 53% toward CO_2RR products), representing the highest CO_2 conversion efficiency reported in the literature to date, regardless of the targeted product.[42]

To challenge the general applicability of the PCRL strategy, we applied this approach with a CO-producing sputtered Ag catalyst (Figure S13). The PCRL strategy resulted in selective production of CO with over 75% FE for all current densities up to 100 mA/cm^2. This result demonstrates that the PCRL coupled CEM configuration provides a locally alkaline cathodic environment that is applicable to CO_2RR catalysts, generally.

The high CO_2 conversion achieved with the PCRL approach does not come at the cost of other performance metrics. The cell voltage and faradaic efficiency with the PCRL are similar to those achieved with the conventional AEM cell tested with the same electrodes (Figure S1). Future advances in AEM technology are applicable to the ionomer contained in the PCRL. The major sources of voltage loss for both cells are the thermodynamic potential, the catalyst overpotentials, and the Nernstian pH loss.[7,43] The FE toward C_2H_4 in particular could be improved further by incorporating specialized catalysts, such as polyamine incorporated Cu.[44−46] The energy efficiency of the PCRL system may also be increased further with advances in the CO_2 permeability of the anion exchange ionomers, an active area of research.[29]

A major benefit of high CO_2 conversion is the avoidance of gas separation costs. After passing through the electrolyzer, any substantial CO_2 content in the anode tail gas must be separated and recirculated, and any unreacted CO_2 in the cathode tail gas must be separated from desired gas products. While membrane-based and pressure-swing separation approaches are emerging for C_2H_4/CO_2 separation,[48,49] typical CO_2 removal processes currently rely on a chemical absorption unit, such as monoethanolamine absorption.[19] In the best-case conversion scenarios achieved here, the molar ratio of output CO_2 to produced C_2H_4 was 0.6 in the PCRL case, compared to 12 with the AEM. The 20-fold reduction in CO_2 content of the cell output—most of which was achieved on the anode side—results in dramatic savings in CO_2 separation energy costs (Figure 5). At 2067 kJ/mol of produced C_2H_4, the energy intensity of CO_2 separation from the AEM electrolyzer anode

https://doi.org/10.1021/acsenergylett.1c01122
ACS Energy Lett. 2021, 6, 2952−2959

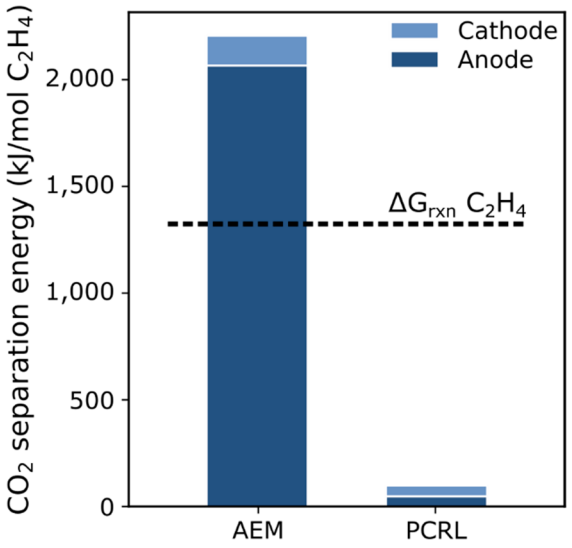

Figure 5. Energy cost for CO_2 separation. A comparison of the energy cost required for downstream CO_2 separation from the cathode and anode gas product streams for an electrolyzer with an AEM and a PCRL-coupled CEM. The C_2H_4 Gibbs free energy of reaction (1331 kJ/mol) is shown for reference. A CO_2 capture energy intensity of 178.3 kJ/mol_CO_2 was applied, based on amine-based capture of CO_2 from flue gas.[47]

output stream surpasses the Gibbs free energy of the reaction, rendering the conventional AEM approach untenable. The PCRL approach provides a solution to the CO_2 conversion challenge and a way forward for the electrocatalytic conversion of CO_2.

We developed a membrane electrode assembly that achieves high single pass conversion of CO_2. The approach blocks CO_2 transport to the anode by locally neutralizing and regenerating the carbonate and bicarbonate anions and enabling transport of regenerated CO_2 from the membrane junction back to the cathode catalyst. Through the optimization of this layer, we demonstrated production metrics (40% and 55% FE toward C_2H_4 and C_{2+} products, respectively, at currents greater than 100 mA/cm^2) competitive with the conventional AEM approach and achieved a near-complete single-pass CO_2 conversion efficiency of 85%. This approach circumvents the fundamental limits of 25% (C_2H_4) and 50% (CO) for AEM-based CO_2 electrolysis. The approach demonstrated here provides a solution to the basic problem limiting the field of electrocatalytic conversion of CO_2 to multicarbon products.

■ ASSOCIATED CONTENT

Supporting Information

The Supporting Information is available free of charge at https://pubs.acs.org/doi/10.1021/acsenergylett.1c01122.

Experimental methods; one-dimensional modeling; faradaic efficiency and cell voltage of the AEM MEA; CO_2 conversion efficiency with and without carbonate formation in the AEM MEA; current density of a CEM MEA; anode gas CO_2 flow with a forward bias BPM MEA; SEM images of the PCRL; structure of a polymer similar to the PCRL; operando ohmic resistance of the PCRL cell; modeled pH at the cathode catalyst; faradaic efficiency of PCRL MEA by loading; PCRL CO_2 conversion with varying current densities; gas velocity and Reynolds number of the flow; stability; faradaic efficiency; and current density of the PCRL coating on an Ag catalyst (PDF)

■ AUTHOR INFORMATION

Corresponding Author

David Sinton − *Department of Mechanical and Industrial Engineering, University of Toronto, Toronto, Ontario M5S 3G8, Canada;* orcid.org/0000-0003-2714-6408; Email: sinton@mie.utoronto.ca

Authors

Colin P. O'Brien − *Department of Mechanical and Industrial Engineering, University of Toronto, Toronto, Ontario M5S 3G8, Canada*

Rui Kai Miao − *Department of Mechanical and Industrial Engineering, University of Toronto, Toronto, Ontario M5S 3G8, Canada*

Shijie Liu − *Department of Mechanical and Industrial Engineering, University of Toronto, Toronto, Ontario M5S 3G8, Canada*

Yi Xu − *Department of Mechanical and Industrial Engineering, University of Toronto, Toronto, Ontario M5S 3G8, Canada;* orcid.org/0000-0002-8108-0975

Geonhui Lee − *Department of Electrical and Computer Engineering, University of Toronto, Toronto, Ontario M5S 1A4, Canada*

Anthony Robb − *Department of Mechanical and Industrial Engineering, University of Toronto, Toronto, Ontario M5S 3G8, Canada*

Jianan Erick Huang − *Department of Electrical and Computer Engineering, University of Toronto, Toronto, Ontario M5S 1A4, Canada*

Ke Xie − *Department of Electrical and Computer Engineering, University of Toronto, Toronto, Ontario M5S 1A4, Canada*

Koen Bertens − *Department of Electrical and Computer Engineering, University of Toronto, Toronto, Ontario M5S 1A4, Canada;* orcid.org/0000-0002-2701-1397

Christine M. Gabardo − *Department of Mechanical and Industrial Engineering, University of Toronto, Toronto, Ontario M5S 3G8, Canada;* orcid.org/0000-0002-9456-6894

Jonathan P. Edwards − *Department of Mechanical and Industrial Engineering, University of Toronto, Toronto, Ontario M5S 3G8, Canada;* orcid.org/0000-0003-4000-5802

Cao-Thang Dinh − *Department of Chemical Engineering, Queen's University, Kingston, Ontario K7L 3N6, Canada;* orcid.org/0000-0001-9641-9815

Edward H. Sargent − *Department of Electrical and Computer Engineering, University of Toronto, Toronto, Ontario M5S 1A4, Canada;* orcid.org/0000-0003-0396-6495

Complete contact information is available at: https://pubs.acs.org/10.1021/acsenergylett.1c01122

Author Contributions

‖Authors contributed equally

Author Contributions

D.S. and E.H.S. supervised the project. C.P.O. and R.K.M. designed and carried out all experiments, as well as prepared the manuscript. S.L. performed the one-dimensional species transport model. Y.X., G.L., and A.R. assisted in experimental setup and data analysis. J.E.H. prepared the Cu electrodes. K.X.

https://doi.org/10.1021/acsenergylett.1c01122
ACS Energy Lett. 2021, 6, 2952−2959

and K.B. performed sample characterization. C.M.G., C-T.D., D.S., and E.H.S. contributed to manuscript editing. J.P.E. aided in the separation analysis. All authors discussed the results and assisted during the manuscript preparation. The authors acknowledge Centre for Nanostructure Imaging at the University of Toronto and Dr. Ilya Gourevich for sample SEM characterization.

Notes

The authors declare the following competing financial interest(s): There is a patent application pending on the PCRL MEA structure described here, filed by the authors of this paper and their institutions.

■ ACKNOWLEDGMENTS

The authors acknowledge support and infrastructure from the Natural Sciences and Engineering Research Council (NSERC), the Government of Ontario, through the Ontario Research Fund. The opinions, results and conclusions are those of the authors, and no endorsement by the Province of Ontario is inferred. C.P.O. thanks the NSERC for their funding toward graduate scholarships. R.K.M. thanks NSERC, Hatch, and the Government of Ontario for their support through graduate scholarships.

■ REFERENCES

(1) Whipple, D. T.; Kenis, P. J. A. A. Prospects of CO2 Utilization via Direct Heterogeneous Electrochemical Reduction. *J. Phys. Chem. Lett.* **2010**, *1* (24), 3451−3458.

(2) De Luna, P.; Hahn, C.; Higgins, D.; Jaffer, S. A.; Jaramillo, T. F.; Sargent, E. H. What Would It Take for Renewably Powered Electrosynthesis to Displace Petrochemical Processes? *Science (Washington, DC, U. S.)* **2019**, *364* (6438), eaav3506.

(3) Bushuyev, O. S.; De Luna, P.; Dinh, C. T.; Tao, L.; Saur, G.; van de Lagemaat, J.; Kelley, S. O.; Sargent, E. H. What Should We Make with CO2 and How Can We Make It? *Joule* **2018**, *2* (5), 825−832.

(4) Verma, S.; Kim, B.; Jhong, H. R. M.; Ma, S.; Kenis, P. J. A. A Gross-Margin Model for Defining Technoeconomic Benchmarks in the Electroreduction of CO2. *ChemSusChem* **2016**, *9* (15), 1972−1979.

(5) Jouny, M.; Luc, W.; Jiao, F. General Techno-Economic Analysis of CO2 Electrolysis Systems. *Ind. Eng. Chem. Res.* **2018**, *57* (6), 2165−2177.

(6) Kutz, R. B.; Chen, Q.; Yang, H.; Sajjad, S. D.; Liu, Z.; Masel, I. R. Sustainion Imidazolium-Functionalized Polymers for Carbon Dioxide Electrolysis. *Energy Technol.* **2017**, *5* (6), 929−936.

(7) Gabardo, C. M.; O'Brien, C. P.; Edwards, J. P.; McCallum, C.; Xu, Y.; Dinh, C. T.; Li, J.; Sargent, E. H.; Sinton, D. Continuous Carbon Dioxide Electroreduction to Concentrated Multi-Carbon Products Using a Membrane Electrode Assembly. *Joule* **2019**, *3* (11), 2777−2791.

(8) Vennekötter, J. B.; Scheuermann, T.; Sengpiel, R.; Wessling, M. The Electrolyte Matters: Stable Systems for High Rate Electrochemical CO2 Reduction. *J. CO2 Util.* **2019**, *32*, 202−213.

(9) Liang, S.; Altaf, N.; Huang, L.; Gao, Y.; Wang, Q. Electrolytic Cell Design for Electrochemical CO2 Reduction. *J. CO2 Util.* **2020**, *35*, 90−105.

(10) Weng, L.-C. C.; Bell, A. T.; Weber, A. Z. Towards Membrane-Electrode Assembly Systems for CO2 Reduction: A Modeling Study. *Energy Environ. Sci.* **2019**, *12* (6), 1950−1968.

(11) Verma, S.; Lu, X.; Ma, S.; Masel, R. I.; Kenis, P. J. A. The Effect of Electrolyte Composition on the Electroreduction of CO2 to CO on Ag Based Gas Diffusion Electrodes. *Phys. Chem. Chem. Phys.* **2016**, *18* (10), 7075−7084.

(12) Dinh, C.-T.; Burdyny, T.; Kibria, M. G.; Seifitokaldani, A.; Gabardo, C. M.; Garcia de Arquer, F. P.; Kiani, A.; Edwards, J. P.; De Luna, P.; Bushuyev, O. S.; Zou, C.; Quintero-Bermudez, R.; Pang, Y.; Sinton, D.; Sargent, E. H. CO2 Electroreduction to Ethylene via Hydroxide-Mediated Catalysis at an Abrupt Interface. *Science (Washington, DC, U. S.)* **2018**, *360*, 783−787.

(13) Xu, Y.; Edwards, J. P.; Liu, S.; Miao, R. K.; Huang, J. E.; Gabardo, C. M.; O'Brien, C. P.; Li, J.; Sargent, E. H.; Sinton, D. Self-Cleaning CO2 Reduction Systems: Unsteady Electrochemical Forcing Enables Stability. *ACS Energy Lett.* **2021**, *6* (2), 809−815.

(14) Voice, A. K.; Rochelle, G. T. Oxidation of Amines at Absorber Conditions for CO2 Capture from Flue Gas. *Energy Procedia* **2011**, *4*, 171−178.

(15) Patru, A.; Binninger, T.; Pribyl, B.; Schmidt, T. J. Design Principles of Bipolar Electrochemical Co-Electrolysis Cells for Efficient Reduction of Carbon Dioxide from Gas Phase at Low Temperature. *J. Electrochem. Soc.* **2019**, *166* (2), F34−F43.

(16) Larrazábal, G. O.; Strøm-Hansen, P.; Heli, J. P.; Zeiter, K.; Therkildsen, K. T.; Chorkendorff, I.; Seger, B. Analysis of Mass Flows and Membrane Cross-over in CO2 Reduction at High Current Densities in an MEA-Type Electrolyzer. *ACS Appl. Mater. Interfaces* **2019**, *11* (44), 41281−41288.

(17) Rabinowitz, J. A.; Kanan, M. W. The Future of Low-Temperature Carbon Dioxide Electrolysis Depends on Solving One Basic Problem. *Nat. Commun.* **2020**, *11* (1), 10−12.

(18) Greenblatt, J. B.; Miller, D. J.; Ager, J. W.; Houle, F. A.; Sharp, I. D. The Technical and Energetic Challenges of Separating (Photo)Electrochemical Carbon Dioxide Reduction Products. *Joule* **2018**, *2* (3), 381.

(19) Aaron, D.; Tsouris, C. Separation of CO2 from Flue Gas: A Review. *Sep. Sci. Technol.* **2005**, *40* (1−3), 321−348.

(20) Ma, M.; Kim, S.; Chorkendorff, I.; Seger, B. Role of Ion-Selective Membranes in the Carbon Balance for CO2electroreduction: Via Gas Diffusion Electrode Reactor Designs. *Chem. Sci.* **2020**, *11* (33), 8854−8861.

(21) Aeshala, L. M.; Rahman, S. U.; Verma, A. Effect of Solid Polymer Electrolyte on Electrochemical Reduction of CO 2. *Sep. Purif. Technol.* **2012**, *94*, 131−137.

(22) Dewulf, D. W.; Bard, A. J. The Electrochemical Reduction of CO2 to CH4 and C2H4 at Cu/Nafion Electrodes (Solid Polymer Electrolyte Structures). *Catal. Lett.* **1988**, *1* (1−3), 73−79.

(23) Komatsu, S.; Tanaka, M.; Okumura, A.; Kungi, A. Preparation of Cu Solid Polymer Electrolyte Composite Electrodes and Application to Gas-Phase Electrochemical Reduction of CO2. *Electrochim. Acta* **1995**, *40* (6), 745−753.

(24) Kim, B.; Ma, S.; Molly Jhong, H.-R.; Kenis, P. J. A. Influence of Dilute Feed and PH on Electrochemical Reduction of CO2 to CO on Ag in a Continuous Flow Electrolyzer. *Electrochim. Acta* **2015**, *166*, 271−276.

(25) Delacourt, C.; Ridgway, P. L.; Kerr, J. B.; Newman, J. Design of an Electrochemical Cell Making Syngas (CO+ H2) from CO2 and H2O Reduction at Room Temperature. *J. Electrochem. Soc.* **2008**, *155* (1), B42−B49.

(26) Li, Y. C.; Zhou, D.; Yan, Z.; Gonçalves, R. H.; Salvatore, D. A.; Berlinguette, C. P.; Mallouk, T. E. Electrolysis of CO2 to Syngas in Bipolar Membrane-Based Electrochemical Cells. *ACS Energy Lett.* **2016**, *1* (6), 1149−1153.

(27) Salvatore, D. A.; Weekes, D. M.; He, J.; Dettelbach, K. E.; Li, Y. C.; Mallouk, T. E.; Berlinguette, C. P. Electrolysis of Gaseous CO2 to CO in a Flow Cell with a Bipolar Membrane. *ACS Energy Lett.* **2018**, *3* (1), 149−154.

(28) Varcoe, J. R.; Atanassov, P.; Dekel, D. R.; Herring, A. M.; Hickner, M. A.; Kohl, P. A.; Kucernak, A. R.; Mustain, W. E.; Nijmeijer, K.; Scott, K.; Xu, T.; Zhuang, L. Anion-Exchange Membranes in Electrochemical Energy Systems. *Energy Environ. Sci.* **2014**, *7* (10), 3135−3191.

(29) Salvatore, D. A.; Gabardo, C. M.; Reyes, A.; O'Brien, C. P.; Holdcroft, S.; Pintauro, P.; Bahar, B.; Hickner, M.; Bae, C.; Sinton, D.; Sargent, E. H.; Berlinguette, C. P. Designing Anion Exchange Membranes for CO2 Electrolysers. *Nat. Energy* **2021**, *6* (4), 339−348.

(30) Oener, S. Z.; Twight, L. P.; Lindquist, G. A.; Boettcher, S. W. Thin Cation-Exchange Layers Enable High- Current-Density Bipolar

https://doi.org/10.1021/acsenergylett.1c01122
ACS Energy Lett. 2021, 6, 2952−2959

Membrane Electrolyzers via Improved Water Transport. *ACS Energy Lett.* **2021**, *6*, 1−8.
(31) Waegele, M. M.; Gunathunge, C. M.; Li, J.; Li, X. How Cations Affect the Electric Double Layer and the Rates and Selectivity of Electrocatalytic Processes. *J. Chem. Phys.* **2019**, *151* (16), 160902.
(32) Murata, A.; Hori, Y. Product Selectivity Affected by Cationic Species in Electrochemical Reduction of CO2 and CO at a Cu Electrode. *Bull. Chem. Soc. Jpn.* **1991**, *64*, 123−127.
(33) Singh, M. R.; Kwon, Y.; Lum, Y.; Ager, J. W.; Bell, A. T. Hydrolysis of Electrolyte Cations Enhances the Electrochemical Reduction of CO2 over Ag and Cu. *J. Am. Chem. Soc.* **2016**, *138*, 13006−13012.
(34) Li, J.; Li, X.; Gunathunge, C. M.; Waegele, M. M. Hydrogen Bonding Steers the Product Selectivity of Electrocatalytic CO Reduction. *Proc. Natl. Acad. Sci. U. S. A.* **2019**, *116* (19), 9220−9229.
(35) Rosen, B. A.; Salehi-Khojin, A.; Thorson, M. R.; Zhu, W.; Whipple, D. T.; Kenis, P. J. A.; Masel, R. I. Ionic Liquid − Mediated Selective Conversion of CO 2 to CO At. *Science (Washington, DC, U. S.)* **2011**, *334*, 643−644.
(36) Asadi, M.; Kim, K.; Liu, C.; Addepalli, A. V.; Abbasi, P.; Yasaei, P.; Phillips, P.; Behranginia, A.; Cerrato, J. M.; Haasch, R.; Zapol, P.; Kumar, B.; Klie, R. F.; Abiade, J.; Curtiss, L. A.; Salehi-Khojin, A. Nanostructured Transition Metal Dichalcogenide Electrocatalysts for CO2 Reduction in Ionic Liquid. *Science (Washington, DC, U. S.)* **2016**, *353* (6298), 467−470.
(37) Sun, L.; Ramesha, G. K.; Kamat, P. V.; Brennecke, J. F. Switching the Reaction Course of Electrochemical CO2 Reduction with Ionic Liquids. *Langmuir* **2014**, *30* (21), 6302−6308.
(38) Grills, D. C.; Matsubara, Y.; Kuwahara, Y.; Golisz, S. R.; Kurtz, D. A.; Mello, B. A. Electrocatalytic CO2 Reduction with a Homogeneous Catalyst in Ionic Liquid: High Catalytic Activity at Low Overpotential. *J. Phys. Chem. Lett.* **2014**, *5* (11), 2033−2038.
(39) Lim, H. K.; Kim, H. The Mechanism of Room-Temperature Ionic-Liquid-Based Electrochemical CO2 Reduction: A Review. *Molecules* **2017**, *22* (4), 536.
(40) Xu, Y.; Edwards, J. P.; Zhong, J.; O'Brien, C. P.; Gabardo, C. M.; McCallum, C.; Li, J.; Dinh, C. T.; Sargent, E. H.; Sinton, D. Oxygen-Tolerant Electroproduction of C2 Products from Simulated Flue Gas. *Energy Environ. Sci.* **2020**, *13* (2), 554−561.
(41) García de Arquer, F. P.; Dinh, C. T.; Ozden, A.; Wicks, J.; McCallum, C.; Kirmani, A. R.; Nam, D. H.; Gabardo, C.; Seifitokaldani, A.; Wang, X.; Li, Y. C.; Li, F.; Edwards, J.; Richter, L. J.; Thorpe, S. J.; Sinton, D.; Sargent, E. H. CO2 Electrolysis to Multicarbon Products at Activities Greater than 1 A Cm-2. *Science (Washington, DC, U. S.)* **2020**, *367* (6478), 661−666.
(42) Dinh, C. T.; Li, Y. C.; Sargent, E. H. Boosting the Single-Pass Conversion for Renewable Chemical Electrosynthesis. *Joule* **2019**, *3* (1), 13−15.
(43) Salvatore, D.; Berlinguette, C. P. Voltage Matters When Reducing CO2 in an Electrochemical Flow Cell. *ACS Energy Lett.* **2020**, *5* (1), 215−220.
(44) Ma, W.; Xie, S.; Liu, T.; Fan, Q.; Ye, J.; Sun, F.; Jiang, Z.; Zhang, Q.; Cheng, J.; Wang, Y. Electrocatalytic Reduction of CO2 to Ethylene and Ethanol through Hydrogen-Assisted C−C Coupling over Fluorine-Modified Copper. *Nat. Catal.* **2020**, *3* (6), 478−487.
(45) Chen, X.; Chen, J.; Alghoraibi, N. M.; Henckel, D. A.; Zhang, R.; Nwabara, U. O.; Madsen, K. E.; Kenis, P. J. A.; Zimmerman, S. C.; Gewirth, A. A. Electrochemical CO2-to-Ethylene Conversion on Polyamine-Incorporated Cu Electrodes. *Nat. Catal.* **2021**, *4* (1), 20−27.
(46) Li, F.; Thevenon, A.; Rosas-Hernández, A.; Wang, Z.; Li, Y.; Gabardo, C. M.; Ozden, A.; Dinh, C. T.; Li, J.; Wang, Y.; Edwards, J. P.; Xu, Y.; McCallum, C.; Tao, L.; Liang, Z. Q.; Luo, M.; Wang, X.; Li, H.; O'Brien, C. P.; Tan, C. S.; Nam, D. H.; Quintero-Bermudez, R.; Zhuang, T. T.; Li, Y. C.; Han, Z.; Britt, R. D.; Sinton, D.; Agapie, T.; Peters, J. C.; Sargent, E. H. Molecular Tuning of CO2-to-Ethylene Conversion. *Nature* **2020**, *577* (7791), 509−513.
(47) Ho, M. T.; Allinson, G. W.; Wiley, D. E. Reducing the Cost of CO2 Capture from Flue Gases Using Pressure Swing Adsorption. *Ind. Eng. Chem. Res.* **2008**, *47*, 4883−4890.
(48) Chen, K. J.; Madden, D. G.; Mukherjee, S.; Pham, T.; Forrest, K. A.; Kumar, A.; Space, B.; Kong, J.; Zhang, Q. Y.; Zaworotko, M. J. Synergistic Sorbent Separation for One-Step Ethylene Purification from a Four-Component Mixture. *Science (Washington, DC, U. S.)* **2019**, *366* (6462), 241−246.
(49) Ebadi Amooghin, A.; Mashhadikhan, S.; Sanaeepur, H.; Moghadassi, A.; Matsuura, T.; Ramakrishna, S. Substantial Breakthroughs on Function-Led Design of Advanced Materials Used in Mixed Matrix Membranes (MMMs): A New Horizon for Efficient CO 2 Separation. *Prog. Mater. Sci.* **2019**, *102*, 222−295.

https://doi.org/10.1021/acsenergylett.1c01122
ACS Energy Lett. 2021, 6, 2952−2959